stress parallel to the Burgers vector in the slip plane but by other stress components. Thus, the deformation behavior of materials with nonplanar dislocation cores may be very complex, often displaying unusual orientation dependencies and breakdown of the Schmid law. The nonplanar dislocation cores are the more common the more complex is the crystal structure, and thus these cores are more prevalent than planar cores. In this respect, f.c.c. materials (and also some hexagonal close-packed (h.c.p.) materials with basal slip) in which the dislocations possess planar cores and, consequently, the Peierls stress is very low, are a special case rather than a prototype for more complex structures.

Additional complex features of the dislocation core structures arise in covalent crystals where the breaking and/or readjustment of the bonds in the core region may be responsible for a high lattice friction stress, and in ionic solids where the cores can be charged which then strongly affects the dislocation mobility. Such dislocation cores affect not only the plastic behavior but also electronic and/or optical properties of covalently bonded semiconductors and ionically bonded ceramic materials.

See also: Mechanical Properties: Anelasticity; Mechanical Properties: Creep; Mechanical Properties: Elastic Behavior; Mechanical Properties: Fatigue; Mechanical Properties: Plastic Behavior; Mechanical Properties: Strengthening Mechanisms in Metals; Mechanical Properties: Tensile Properties; Periodicity and Lattices; Recovery, Recrystallization, and Grain Growth; Thin Films, Mechanical Behavior of.

PACS: 61.72.Fp; 61.72.Hh; 61.72.Lk; 72.10.Fk

Further Reading

Colonnetti G (1915) *Accadutti. Licwinaz R. C.* 24: 404.
Eshelby JD (1956) In: Seitz F and Turnbull D (eds.) *Solid State Physics*, vol. 3, p. 79. New York: Academic Press.
Friedel J (1964) *Dislocations*. Oxford: Pergamon.
Hirth JP and Lothe J (1982) *Theory of Dislocations*, 2nd edn. New York: Wiley.
Hull D and Bacon DJ (2001) *Introduction to Dislocations*. Oxford: Butterworth-Heinemann.
Khantha M, Pope DP, and Vitek V (1994) *Physical Review Letters* 73: 684.
Kléman M and Lavrentovich OD (2003) *Soft Matter Physics: An Introduction*. New York: Springer.
Kosterlitz JM and Thouless DJ (1973) *Journal of Physics C: Solid State Physics*. 6: 1181.
Lardner RW (1974) *Mathematical Theory of Dislocations and Fracture*. Toronto: University of Toronto Press.
Nabarro FRN (1967) *Theory of Crystal Dislocations*. Oxford: Clarendon Press.
Orowaon E (1934) *Zeitschrift für Physik* 89: 634.
Paidar V and Vitek V (2002) In: Westbrook JH and Fleisher RL (eds.) *Intermetallic Compounds: Principles and Practice*, vol. 3, p. 437. New York: Wiley.
Peach MO and Koehler JS (1950) *Physical Review* 80: 436.
Polanyi M (1934) *Zeitschrift für Physik* 89: 660.
Taylor GI (1934) *Proceedings of Royal Society London A* 145: 362.
Vitek V (2004) *Philosophical Magazine* 84: 415.
Volterra V (1907) *Ann. Sci. Ec. Norm. Sup. Paris* 24: 401.

Disorder and Localization Theory

E N Economou, University of Crete, Greece
C M Soukoulis, Iowa State University, Ames, IA, USA

Introduction

A plane electronic wave, $\exp(i\boldsymbol{k}\cdot\boldsymbol{r})$, impinging upon a local potential, $v(|\boldsymbol{r}-\boldsymbol{r}_n|)$, centered at $\boldsymbol{r}_n$, is scattered, thus giving rise to a spherical wave of the form $f(\theta,\phi)\exp(i\boldsymbol{k}\cdot\boldsymbol{r})/r$ as $r\to\infty$. The scattering amplitude, f, is related to the differential $d\sigma/d\Omega(=|f(\theta,\phi)|^2)$, and the total scattering cross section, σ. The total scattering cross section, $\sigma=\int|f|^2\,d\Omega$, gives essentially the part of the area of the incoming wave front intercepted by the scattering potential. For transport properties, the relevant cross section is $\sigma_t=\int(1-\cos\theta)|f|^2\,d\Omega$.

An electron propagating within a solid or liquid is subject to many local scattering potentials stemming from the atoms comprising the solid or liquid, and giving rise to a total scattering potential $V(\boldsymbol{r})=\sum_n v(|\boldsymbol{r}-\boldsymbol{r}_n|)$. The response of electrons to $V(\boldsymbol{r})$ is of central importance in understanding and controlling the mechanical, electrical, magnetic, and optical properties of materials.

Identical and periodically placed scatterers allow a systematic constructive interference of the scattered waves, which to a great extent, compensates the effects of the scattering. As a result, a periodic potential, $V(\boldsymbol{r})$, produces plane-wave-like solutions, called Bloch waves, of the form $u_{kj}(\boldsymbol{r})\exp[i(\boldsymbol{k}\cdot\boldsymbol{r}-\omega_{kj}t)]$, associated with bands of allowed values of ω_{kj}; u_{kj} is a periodic function of $\boldsymbol{r}$ with the same period as $V(\boldsymbol{r})$. Gaps in the spectrum also appear because of systematic destructive interference (another effect of

periodicity) and/or well-separated atomic or molecular levels giving rise to nonoverlapping bands.

"Classical" Treatment of Disorder

In actual solids, there are always static, chemical and, structural deviations from periodicity, located randomly within the solid; in other words, there is always disorder. The thermal vibrations of atoms (or ions), although dynamical in nature, can be treated for fast processes and high temperatures as additional sources of static disorder. However, at low temperatures, lattice vibrations and other dynamical processes lead to inelastic scatterings, which are clearly distinct from the elastic scatterings considered up to now; these inelastic scatterings are responsible for an energy uncertainty, ΔE, which in turn defines an inelastic dephasing time $\tau_\phi \sim \hbar/\Delta E$; for $t \gtrsim \tau_\phi$, the phase is randomized.

Disorder is crucial in determining important transport properties, such as electrical and thermal conductivities, magnetoresistances, photoconductivities, and metal–insulator transitions. Under normal conditions, the main role of disorder is to change the propagation of electrons (or more generally, of whatever carriers) from ballistic to diffusive; the latter involves a new characteristic quantity, the so-called transport mean free path, l, which is connected to the diffusion length $L_D = (D\tau)^{1/2}$ by the relation $L_D = l/\sqrt{d}$. D is the diffusion coefficient, $\tau = l/v$, v is the carrier velocity, and d is the space dimensionality. The transport mean free path, for low concentration, $n_s = N_s/V$, of scatterers is related to the transport cross section σ_{ti} of each scatterer by the relation

$$\frac{1}{l} = \frac{1}{V}\sum_{i=1}^{N_s} \sigma_{ti} \qquad [1]$$

which means that over a length l, the N_s scatterers within the volume $V = Sl$ will intercept the whole cross section, S, of the incoming wave (i.e., $S = \sum_i \sigma_{ti}$).

The summation of σ_{ti}s in eqn [1] implies that interference effects have been omitted; thus the term "classical" in the title of this subsection. Actually, a scattered wave from one scatterer can be scattered again by other scatterers; this is especially true when the σ_{ti}s are large and their concentration, n_s, is high. All these single and multiple scattered waves can, in principle, interfere with one another, possibly modifying the basic result in eqn [1]. The argument in support of eqn [1] is that constructive and destructive interference more or less cancel each other as a result of the interfering waves having random phase differences (associated with the random positions and phase shifts of the scatterers).

Weak Disorder and the Role of Interferences

Consider an electron initially ($t = 0$) at the point $\boldsymbol{r}$. The probability density amplitude, $A(t)$, to again find the electron at $\boldsymbol{r}$, after time t, is given by $A(t) = \sum_v A_v(t)$, where the sum is over all directed path integrals, $A_v = \exp[(i/\hbar)\int_0^t L(\boldsymbol{r}_v(t'))\,dt']$, starting and ending at $\boldsymbol{r}$. The probability density, $dP(t)/d^3r$, to find the electron at $\boldsymbol{r}$ after time t is $dP/d^3r = |A(t)|^2 = \sum_v |A_v(t)|^2 + \sum_{v\neq\mu} A_v(t)A_\mu^*(t)$. Omitting the last double sum on the basis of random phases is equivalent to the approximation leading to eqn [1]. However, not all terms with $\mu \neq v$ have random phases; indeed, for each path $\mu = \bar{v}$, where $\bar{v}$ is the same as path v but run in the opposite direction, $A_\mu = A_{\bar{v}} = A_v$ (the last equality stems from time-reversal symmetry), and consequently $\sum_{v\neq\mu} A_v A_\mu^* = \sum_v A_v A_{\bar{v}}^* + \sum_{\mu\neq v,\bar{v}} A_v A_\mu^*$. Thus, making the reasonable assumption that $\sum_{\mu\neq v,\bar{v}} A_v A_\mu^*$ is really zero because of random phases, one may come to the conclusion that dP/d^3r is twice as big as the classical diffusion would predict, since $\sum_v A_v A_{\bar{v}}^* = \sum_v |A_v|^2$. Actually, $dP(t)/d^3r$ is less than twice as large because the equality $A_{\bar{v}} = A_v$ is not valid for very long paths, whose length far exceeds the inelastic dephasing length $L_\phi \equiv (D\tau_\phi)^{1/2}$; for such long paths, repeated inelastic scattering destroys the phase equality of $A_{\bar{v}}$ and A_v. In any case, the conclusion is that interference effects make quantum diffusion slower than classical diffusion, and lead to a decrease of the diffusion coefficient and the electrical conductivity. This decrease is proportional to the integral $\int dt \sum_v A_v A_{\bar{v}}^*$.

The latter can be estimated by taking into account that the paths which contribute are inside a tube of cross section λ^2 (or λ^{d-1} for a d-dimensional system, where λ is the wavelength) around the classical trajectory. Furthermore, the probability of returning is directly related to the probability of self-intersection of this orbital tube. Within time dt, the wave would move by $v\,dt$ and would sweep a volume $dV = \lambda^{d-1} v\,dt$; hence, the probability of self-intersection during the time interval dt, after time t has elapsed, is equal to the ratio of the volume $dV = \lambda^{d-1} v\,dt$ over the total volume swept up to t; the latter is of the order of $L_D^d = (Dt)^{d/2}$. Hence, the probability of self-intersection at any time between $t = \tau$ and $t = \tau_\phi$ is proportional to $\int_\tau^{\tau_\phi} dt \lambda^{d-1} v/(Dt)^{d/2}$. The elastic collision time, $\tau = l/v$, has been set as the lower limit because, for $t \ll \tau$, the motion is ballistic and the probability of self-intersection is zero; the inelastic dephasing time τ_ϕ is the upper limit since for $t \gtrsim \tau_\phi$,

the phase equality of A_v and $A_{\bar{v}}$ is lost. Notice that at high temperatures, where $\tau_\phi \approx \tau$, the quantum corrections are negligible. On the other hand, for low temperatures, where $\tau_\phi \gg \tau$, there is an appreciable increase in the probability, p, of returning to the initial point and consequently an appreciable correction, $\delta\sigma = \sigma - \sigma_0$, to the classical conductivity, σ_0, as a result of interference effects:

$$\delta\sigma \sim -p \sim 1 - \left(\frac{\tau_\phi}{\tau}\right)^{1/2} \approx -\left(\frac{\tau_\phi}{\tau}\right)^{1/2} = -\frac{L_\phi}{L_D} \text{ (1D systems)} \quad [2a]$$

$$\delta\sigma \sim -p \sim -\frac{\lambda}{L_D}\ln\frac{\tau_\phi}{\tau} = -\frac{2\lambda}{L_D}\ln\frac{L_\phi}{L_D} \text{ (2D systems)} \quad [2b]$$

$$\delta\sigma \sim -p \sim -\frac{\lambda^2}{L_D^2}\left[1 - \left(\frac{\tau}{\tau_\phi}\right)^{1/2}\right] = -\frac{\lambda^2}{L_D^2}\left(1 - \frac{L_D}{L_\phi}\right) \approx 0 \text{ (3D systems)} \quad [2c]$$

The above formulas are valid when the disorder is weak, so that $|\delta\sigma|$ is considerably smaller than σ_0, since otherwise, one could end up with negative conductivity $\sigma = \sigma_0 + \delta\sigma$. The condition $|\delta\sigma| \ll \sigma_0$ implies that $\lambda \ll L_D$, which in turn means that under the present conditions, $\delta\sigma$ is negligible for 3D systems. On the other hand, for 1D and 2D systems, $\delta\sigma$ can become appreciable when $L_\phi \gg L_D$; furthermore, since τ_ϕ is proportional to T^{-1} for 2D and $T^{-2/3}$ for 1D systems, and for very low temperatures, T, it follows that σ for $d = 1$ and $d = 2$ decreases with decreasing T. Such a T-dependence suggests an insulating behavior as $T \to 0$K, and consequently, the nonexistence of one- and two-dimensional metallic behavior. In other words, the possibility is raised that in 1D and 2D systems, as $L_\phi \to \infty$, the conductivity may become zero, no matter how weak the disorder is. The possibility of $\sigma \to 0$ as $L_\phi \to \infty$ may be realized even in 3D systems when the disorder is strong enough, so that $\lambda \gtrsim L_D$. This question is taken up again in the next subsection, in which formulas [2a]–[2c] are generalized to the strong disorder case.

This subsection is concluded by pointing out that the presence of a magnetic field, $\boldsymbol{B}$, breaks the time-reversal symmetry, and as a result, breaks the equality $A_v = A_{\bar{v}}$, and consequently, reduces the magnitude of $|\delta\sigma|$, and thus, tends to restore the classical behavior. Actually, the magnetic field adds a term $q\boldsymbol{A}\cdot\boldsymbol{v}$ to the Lagrangian, where q is the charge of carriers ($-e$ for electrons), and $\boldsymbol{A}$ is the vector potential such that $\boldsymbol{B} = \nabla \times \boldsymbol{A}$. So the closed path integrals, A_v, $A_{\bar{v}}$, in the presence of $\boldsymbol{B}$, acquire an extra phase, that is $A_v = A_{v0}\exp(i\phi_v)$, $A_{\bar{v}} = A_{v0}\exp(-i\phi_v)$, where $\phi_v = q\Phi_v/\hbar$, and Φ_v is the magnetic flux through the closed path. As a result $A_v A_{\bar{v}}^* + A_{\bar{v}} A_{\bar{v}}^* = 2|A_{v0}|^2\cos(2\phi_v)$, instead of $2|A_{v0}|^2$ as in the case $\boldsymbol{B} = 0$. This implies a periodic variation of the conductance as a function of the applied magnetic field if Φ_v is a constant independent of v. Indeed, this phenomenon has been observed in cylindrical tubes of cross section S with very thin walls, and with the magnetic field parallel to the axis of the tube. The configuration is such that $\Phi_v = nBS$, where $n = 1, 2, \ldots$. Because L_ϕ^2 is not much larger than S, the dominant contribution comes from $n = 1$ and the conductance, G, varies as $\delta G \sim \cos(2eBS/\hbar)$; this is the so-called $h/2e$ Aharonov–Bohm effect. In ring configurations, such as in **Figure 1c**, where the conduction paths are between diametrically opposite points, the variation of the conductance, δG, is proportional to $\cos(eBS/\hbar)$; this is the so-called h/e Aharonov–Bohm effect. Notice that the Aharonov–Bohm effects can provide an operational definition of the length L_ϕ, since for lengths $L \gtrsim L_\phi$, the characteristic conductance oscillations gradually disappear. In thin wires, such as in **Figures 1d** and **1e**, the oscillatory magnetic field dependence of the conductance is more complicated as shown in **Figure 2**. It must be pointed out that these oscillations are reproducible (for the same system) and that their size is universal and $\sim e^2/\pi\hbar$. Furthermore, the conductance in the system of **Figure 1d** is different from that in the system of **Figure 1e**, in spite of the classical current carrying paths being identical in the two configurations; this shows the wave nature of electronic propagation, the non-negligible role of interference effects associated with the existence of the ring in **Figure 1e**, and the nonlocal nature of the current–electric field relation.

Disorder, Density of States, and Wave Functions

Three-Dimensional systems

In **Figure 3a**, the density of states (DOS) of a band associated with the s-level of identical atoms placed periodically in a simple cubic lattice is shown; the bandwidth is $12|V_2|$, where V_2 is the matrix element transferring electrons between two neighboring atoms. Disorder is introduced (**Figures 3b–3d**) by assuming that the s-levels of atoms are independent random variables possessing a Gaussian distribution of standard deviation w. The effects of the disorder are the following: (1) The analytical singularities

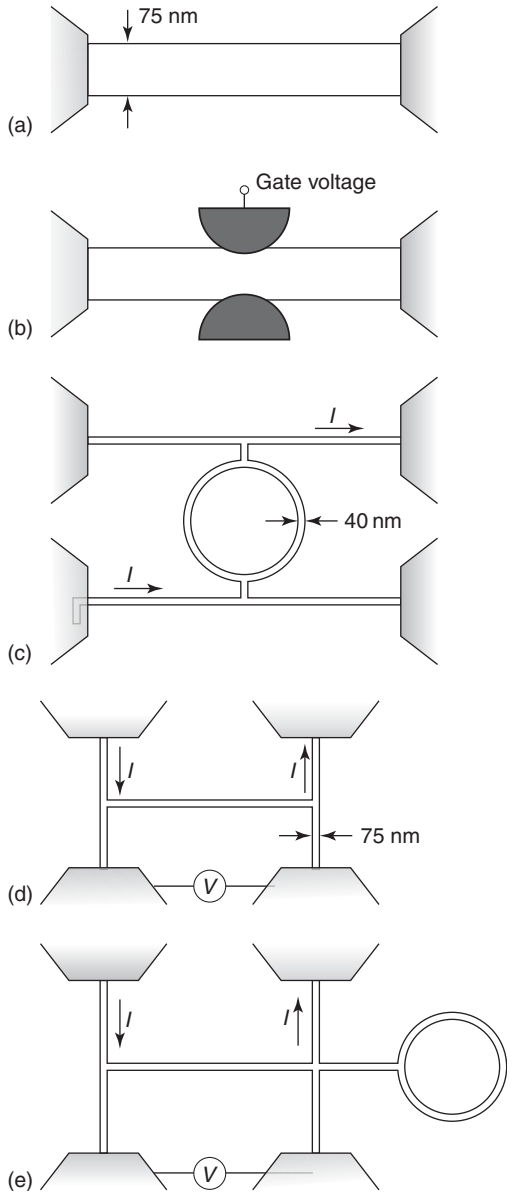

Figure 1 Various mesoscopic wires. (a) Simple quantum wire. (b) The gate voltage, V_G, creates a restriction which gradually, by changing V_G, leads to the 1D limit. (c) Four probe ring configuration which splits the current to the two semicircular paths. (d, e) Four probe configurations differing by the presence of the ring in case (e). The cross sections of the wires are $\sim 10^3\,\text{nm}^2$, and their length $\sim \mu\text{m}$.

shown in **Figure 3a** disappear. (2) The bandwidth increases as the band edges $\pm E_B^{(0)}$ move to new positions $\pm E_B$, where $E_B - E_B^{(0)} = c_1 w^2/|V_2|$ ($c_1 \approx 0.25$ in the present case). (3) Besides this widening of the band, tails in the DOS, $\rho(E)$, appear which are of exponential nature, $\rho(E) \sim \exp(-|E|/E_0)$ for $E_B \lesssim |E|$, where $E_0 = c_2 w^2/|V_2|$ ($c_2 \approx 0.12$ in the present case); these tails give rise to tails in the optical absorption of semiconductors for $\hbar\omega$ less than the gap (Urbach tails). (4) Two characteristic energies, $\pm E_c$, termed mobility edges, appear at which the nature of the eigenstates changes from propagating (or extended) to nonpropagating (or localized, shaded regions in **Figures 3b–3d**). The localized eigenstates are trapped either around a cluster of atoms or around a single atom whose *s*-energy level is much different than the average. For low disorder ($w \lesssim 2.5|V_2|$), the mobility edges follow the band edges closely, $|E_B| - |E_c| \sim w^4/|V_2|^3$. As the disorder increases, the mobility edges start moving toward the center of the band, and eventually they merge together making all eigenstates of the band localized; this is known as the Anderson transition (in the present case, this transition occurs when $w \simeq 6.2|V_2|$).

For weak disorders (e.g., **Figure 3b**), the states near the center of the band are quasi-Bloch characterized by the band index, j, the wave vector, $\boldsymbol{k}$, and the mean free path, which is connected to the phase $\phi(\boldsymbol{r})$ of the eigenfunction through the relation $\langle \exp[i\phi(\boldsymbol{r}) - i\phi(0)] \rangle = \exp(-r/2l')$, where the symbol $\langle\ \rangle$ denotes the average value over all random variables. The mean free path l' satisfies eqn [1] with σ_i instead of σ_{ti}. As one moves from the center of the band toward the mobility edges, the amplitude of the eigenstates develops ever increasing fluctuations, both in magnitude and spatial extent up to a maximum length, ξ; for distances, r, such that $a \ll r \lesssim \xi$, the eigenfunctions exhibit a statistically self-similar, fractal, behavior (a is the lattice spacing). As $|E| \to |E_c|$, ξ blows up, $\xi \to A/(|E_c| - |E|)^\gamma$, where γ has been estimated to be 1.58 (in the absence of a magnetic field) and 1.43 (in the presence of a magnetic field). On the localized sides of the spectrum, the eigenfunctions, $\psi(\boldsymbol{r})$, decay exponentially on the average, that is, $\langle |\psi(\boldsymbol{r})| \rangle_g \sim \exp(-r/L_c)$, as $r \to \infty$, where $\langle |\psi(\boldsymbol{r})| \rangle_g \equiv \exp[\langle \ln|\psi(\boldsymbol{r})| \rangle]$, and L_c is the so-called localization length. For distances, r, such that $a \ll r \lesssim L_c$, the eigenfunctions exhibit fluctuations of statistically self-similar, fractal nature. As $|E| \to |E_c|$, L_c blows up: $L_c \to A'/(|E| - |E_c|)^\gamma$.

The contribution of a band to the conductivity, $\sigma(T)$, is given by $\sigma(T) = \int dE \sigma(E,T)(-\partial f/\partial E)$, where $f(E)$ is the Fermi–Dirac distribution, $\sigma(E,T)$ is proportional to the DOS $\rho(E)$ and the mobility $\mu(E)$ at E. The conductivity $\sigma(E,T)$ for a finite cube of length L at $T = 0\,\text{K}$ is given by

$$\sigma(E,0) = \frac{e^2}{\hbar}\left(\frac{0.066}{\xi} + \frac{A_1}{L}\right) \qquad [3]$$

for E in the extended region (A_1 is ~ 0.05), $\sigma(E,0) \sim \exp(-2L/L_c)$ in the localized regime, and for $L_c \ll L$. Actually, L, besides the length of the specimen, can be of any number of upper cut-off lengths such as L_ϕ or $R_B = (\hbar c/eB)^{1/2}$, the cyclotron

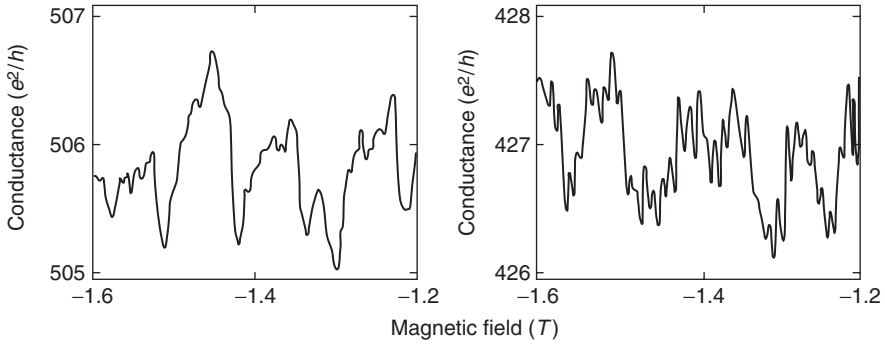

Figure 2 Electrical conductance vs. applied magnetic field for the configuration of **Figure 1d** (left) and for that of **Figure 1e** (right). (Reproduced with permission from Webb RA and Washburn S (1988) Quantum interference fluctuations in disordered metals. *Physics Today* 41: 46; © American Institute of Physics.)

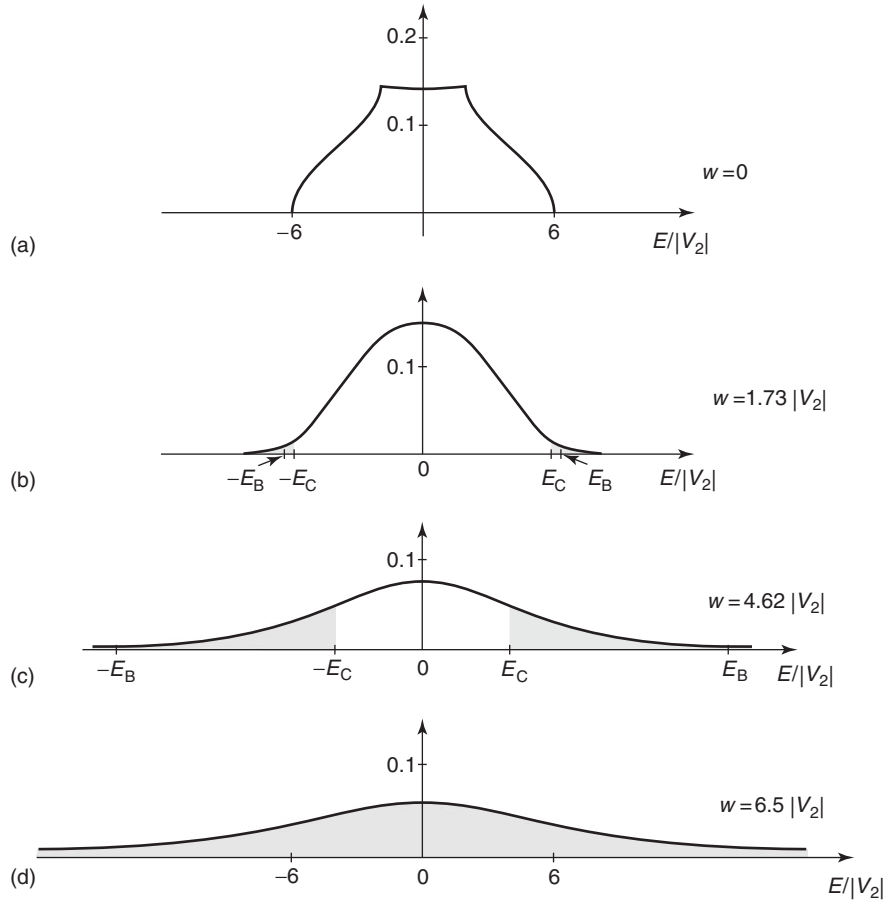

Figure 3 The density of states (DOS) of a band associated with the *s*-level of atoms placed periodically in a simple cubic lattice. The *s*-level of each atom is an independent random variable of Gaussian probability distribution with zero-average value and standard deviation equal to w, which goes from zero (case (a)) to $6.5|V_2|$ (case (d)). The bandwidth at $w = 0$ is $12|V_2|$. Shaded regions correspond to localized eigenstates.

radius in the presence of a magnetic field, or $L_\omega = (D/\omega)^{1/2}$, the diffusion length in the presence of an AC field of frequency ω, etc. In the presence of all these upper cut-off lengths, L in the above formulas should be replaced by an effective length, $\tilde{L}$, probably of the form $\tilde{L}^{-2} = c_1 L^{-2} + c_2 L_\phi^{-2} + c_3 L_\omega^{-2} + c_4 R_B^{-2} + \cdots$, where the weights c_i are of the order of unity.

Two-Dimensional Systems

2D systems, such as very thin films or electrons trapped at the interface of Si/SiO_2 or $GaAs/Al_xGa_{1-x}As$,

are borderline as far as localization properties are concerned. In the absence of magnetic forces, all eigenstates are localized, no matter how weak the disorder is (exceptions do exist). In the presence of magnetic forces, the situation is qualitatively similar to that shown in **Figure 3b–3d** with an extremely narrow region of extended states at the center of the band. This picture has been employed to interpret the so-called integral quantum hall effect (IQHE), where as the Fermi level moves in the localized regime, the Hall resistance does not change until it enters the extended regime and a rather abrupt step is exhibited.

In the absence of magnetic forces, the localization length at E is related to the mean free path $l(E) : L_c(E) \simeq 2.7l(E)\exp[S(E)l(E)/4]$, where $S(E)$ is the length of the line in $\boldsymbol{k}$-space satisfying the equation $E_k = E$. The conductivity $\sigma(E,0)$ is given by an approximate interpolation formula involving $\tilde{L}$ and L_c as well as a length $r_0 \simeq c'l$. In the limit $\tilde{L} \ll L_c$,

$$\sigma \approx \sigma_0 - \frac{e^2}{\pi^2\hbar}\ln\frac{\tilde{L}}{r_0} \qquad [4]$$

while for $L_c \ll \tilde{L}$, $\sigma = (2\sigma_0\tilde{L}/L_c)\exp(-2\tilde{L}/L_c)$. Equation [4] is similar to eqn [2b] and is known as a weak localization correction. For $\tilde{L} \simeq R_B$, eqn [4] gives $\Delta\sigma \equiv \sigma(B) - \sigma(0) = (e^2/2\pi^2\hbar)\ln[1 + (eL_\phi^2 B/1.78\hbar c)]$, that is a negative magnetoresistance, $\Delta R/R \simeq -\Delta\sigma/\sigma$, as shown in **Figure 4**. For $L \simeq L_\phi \sim T^{-1/2}$, the above formulas for the conductivity show that $\sigma \to 0$ as $T \to 0$ K. Notice, however, that electron–electron interactions produce a similar temperature dependence. Nevertheless, recent experiments at very low temperatures, in very clean interfaces $GaAs/Al_xGa_{1-x}As$ or Si/SiO_2, have shown that $\sigma(T)$ stops decreasing and starts increasing with decreasing temperatures.

One-Dimensional and Quasi-One-Dimensional Systems

For 1D systems, such as the one shown in **Figure 1b**, all eigenstates are localized, no matter how small the disorder is (exceptions do exist); the localization length is proportional to the mean free path, $L_c = cl$, where the coefficient c equals 4 for not-so-strong a disorder. The conductivity, σ, is given by $\sigma = (e^2\tilde{L}/\pi\hbar)/[\exp(2\tilde{L}/L_c) - 1]$. Thus in the limit $\tilde{L} \ll L_c$, $\sigma = (e^2L_c/2\pi\hbar) - (e^2\tilde{L}/2\pi\hbar)$; the first term gives the classical result $\sigma = 2e^2l/\pi\hbar$, since $L_c = 4l$, while the second is linear in $\tilde{L}$ as in eqn [2a]. Taking into account that the conductance G in 1D equals to $\sigma/\tilde{L}$ and that the geometrically averaged transmission coefficient, T, equals to $\exp(-2\tilde{L}/L_c)$, the formula for σ can be recast as $G = (e^2/\pi\hbar)T/(1 - T)$. However, a direct calculation of G gives $G = (e^2/\pi\hbar)T$. This discrepancy is due to the fact that the first formula gives the conductance of the wire *per se* without taking into account the two contact resistances $2R_c = \pi\hbar/e^2$, and it requires a four-probe measurement for its determination; on the contrary, the result $G = (e^2/\pi\hbar)T$ is the outcome of a two-probe measurement and it includes the contact resistances, so that $1/G = 2R_c + R_w = (\pi\hbar/e^2) + (\pi\hbar/e^2)[(1 - T)/T] = (\pi\hbar/e^2)/T$. In the presence of M coupled parallel to 1D channels in the limit where $\tilde{L} \ll l$ and $T \simeq 1$, the two-probe measurement will give $G = (e^2/\pi\hbar)M$ in agreement with the experimental results in **Figure 5**. The importance of the above formulas lies in their

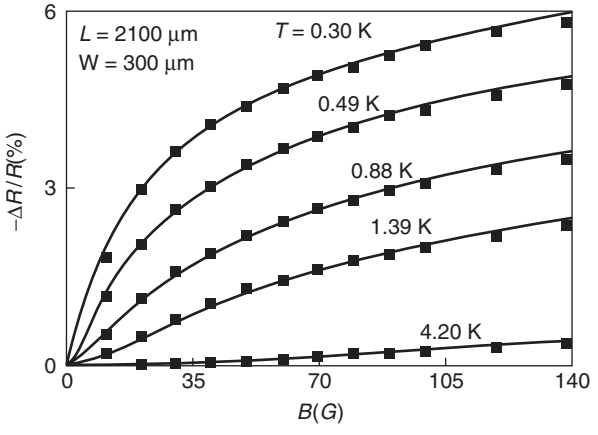

Figure 4 Experimental data (solid squares) and theoretical results (continuous lines) for the relative magnetoresistance $-\Delta R/R$, in a two-dimensional sample of electronic concentration $n = 1.6 \times 10^{11}$ cm^{-2} and mobility $\mu = 27\,000$ cm^2 V^{-1} s^{-1} (Reproduced from Choi KK *et al.* (1987) Dephasing time and one-dimensional localization of two-dimensional electrons in $GaAs/Al_xGa_1 - xAs$ heterostructures. *Physical Review B* 36: 7751.)

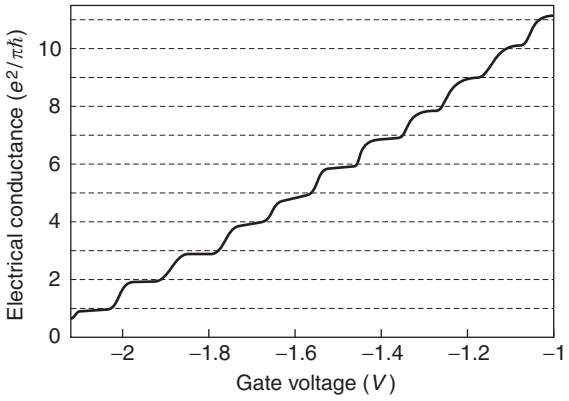

Figure 5 The electrical conductance of the configuration shown in Figure 1b vs. the gate voltage, V_g. The step-like dependence on V_g according to the formula $G = (e^2/\pi\hbar)M$, $M = 1, 2, \ldots$, is shown. For $V_g < -2V$, the 1D limit $M = 1$ has been reached (Reproduced from van Wees BJ *et al.* (1988) Quantized conductance of point contacts in a two-dimensional electron gas. *Physical Review Letters* 60: 848.)

capability to be generalized to a multiterminal system; each terminal, i, is in contact with a reservoir at electrochemical potential $\mu_i = -|e|V_i$, and feeds the system with a net current I_i

$$I_i = \frac{e^2}{\pi\hbar}\sum_i T_{i\leftarrow j}(V_i - V_j) \qquad [5]$$

Equation [5] is very useful in treating many mesoscopic systems, such as quantum dots exhibiting the phenomenon Coulomb blockade.

Justifying the Localization Picture

Several theoretical/numerical methods have been employed to obtain the various localization quantities such as L_c, ξ, E_c, $\delta\sigma$, etc.

Level Statistics

Localized eigenstates belonging to neighboring energy levels of a very large system are, in general, far away from one another and hence, they have negligible overlap and as a result, negligible level repulsion. On the contrary, extended eigenstates always overlap, and thus always exhibit level repulsion. Hence, the probability distribution of the separation of two consecutive energy levels (which can be obtained numerically) is quite different for localized and extended eigenstates. This difference is an efficient way for determining regions of localized and extended states.

Transfer Matrix Techniques

A transfer matrix, t_{12}, propagates the general solution of the wave equation from point x_1 to point x_2 along 1D and quasi-1D systems. By multiplying transfer matrices, $t_{0L} = t_{12}t_{23}\ldots t_{NL}$, the solution at one end $(x = 0)$ can be connected to the solution at the other end $(x = L)$. For disordered quasi-1D systems, the eigenvalues of t_{0L} come in pairs $(\mu_i, \bar{\mu}_i)$, such that $\mu_i \to \exp(L/L_{ci})$ and $\bar{\mu}_i \to \exp(-L/L_{ci})$ as $L \to \infty$, where $\pm L_{ci}^{-1}$ are the so-called Lyapunov exponents. The longest L_{ci}, L_c, determines the transmission coefficient, T, of the quasi-1D system of length L as $T = (-2L/L_c)$. By considering quasi-1D strips of M coupled channels arranged in a plane, or wires of square cross section with M^2 channels, $L_c(M)$ can be determined numerically; by employing a scaling property, the limit $M \to \infty$ can be taken, which determines L_c for the 2D case ($L_c = \lim L_c(M)$ as $M \to \infty$), and both L_c (when $L_c(M)$ converges as $M \to \infty$) and ξ (when $L_c(M) \sim M^2/\xi$) for the 3D case.

Scaling Approach

In the model considered in **Figure 3**, the only relevant parameter is the dimensionless ratio $w/|V_2|$. Then a cluster of p neighboring atoms of length $L_1 = p^{1/d}a$ (where a is the lattice spacing) is examined and one may attempt to define a single dimensionless ratio, Q_1, which would play for the cluster the same role as $w/|V_2|$ plays for each atom. By repeating the rescaling n times, where n eventually approaches infinity, one finds that $Q_n = (\hbar/e^2)G$, where G is the conductance of a d-dimensional "cube" of linear dimension $L = p^{n/d}a$. Since $Q_n \equiv Q(L)$ is the only relevant parameter, the occurrence or not of localization depends on whether $Q(L)$ tends to infinity or to zero respectively, as $L \to \infty$. To find this limit, the logarithmic derivative $\beta = \mathrm{d}\ln Q/\mathrm{d}\ln L$, which depends on the parameter Q, is defined. In the limit $Q \to \infty$, the classical behavior is approached, which gives that $Q \sim G \sim L^{d-2}$; hence $\beta \to d - 2$, that is, negative for $d < 2$ and positive for $d > 2$. Assuming that β is a monotonically increasing function of Q, one can conclude that in the limit $L \to \infty$, $G \to 0$ for $d < 2$. For $d > 2$, $G \to \infty$ as $L \to \infty$ (in the region $\beta > 0$), and $G \to 0$ as $L \to \infty$ (in the region $\beta < 0$).

Potential Well Analogy

More sophisticated approximate analytical approaches for the calculation of σ permit one, under certain conditions, to map the localization question to that of an effective d-dimensional potential well (in the absence of magnetic forces) of depth $V_0(E) \sim [\sigma_0(E)]^{-1}[l(E)]^{-d}$ and linear extent $a \sim l(E)$. If this effective potential well sustains a bound state of decay length $L_c(E)$, then the states at E are localized with localization length equal to $L_c(E)$. If the effective potential well exhibits a resonance in the cross section at $E_r(E)$, then the eigenstates at E are extended with a length ξ given by $E_r(E) = \hbar^2/2m\xi^2(E)$, $\xi \gg l$. Using the fact that a potential well, no matter how shallow, always sustains a bound state for $d \leqslant 2$, while it must exceed a critical value of V_0a^2 to sustain a bound state for $d = 3$, the basic picture presented before is recaptured, before including the expressions for the localization length in 1D and 2D systems. Furthermore, by employing the critical value of V_0a^2, one finds that localized states appear in 3D systems, when the product $lk \lesssim 0.85$ or $l/\lambda \lesssim 0.14$; this is the so-called Ioffe–Regel criterion.

Classical Wave Localization

In addition to the work of electronic localization presented above, the question of classical localization has received attention. This interest is due partly to the fact that classical waves, such as electromagnetic or acoustic/elastic, being subject to destructive

interference and hence to the possibility of localization, can serve as a model system for testing the theory of Anderson localization of electrons experimentally in a clean way, without the complication of strong inelastic scattering and other effects of electron–electron and electron–phonon interactions. On the other hand, it is harder to localize classical waves, mainly due to the fact that at low frequencies, the effects of disorder tend to be wiped out, whereas electrons at low energies are trapped very effectively, even by a weak random potential.

To see this, consider the simple scalar wave equation, $\nabla^2 u + (\omega^2/c^2)u = 0$, where the velocity, $c(\boldsymbol{r})$, in the medium varies from point to point between a maximum, c_M, and a minimum, c_m, value. Compare this equation with Schrödinger's equation in the presence of a potential $V(\boldsymbol{r})$ which varies between V_M and V_m. The two equations are mathematically equivalent if one makes the following correspondences:

$$\frac{\omega^2}{c_M^2} \leftrightarrow \frac{2m}{\hbar^2}(E - V_M) \qquad [6a]$$

$$\omega^2\left(\frac{1}{c_M^2} - \frac{1}{c(\boldsymbol{r})^2}\right) \leftrightarrow \frac{2m}{\hbar^2}[V(\boldsymbol{r}) - V_M] \qquad [6b]$$

Equation [6a] implies that classical waves correspond to electronic waves, but for energy above the maximum value of the potential; eqn [6b] shows that the scattering producing fluctuations in the classical wave case are multiplied by ω^2, and thus are fully ineffective for low frequencies. The conclusion is that classical waves can only be localized, if at all, at intermediate frequencies. The analogies between the classical and quantum problems indeed lead to many cross fertilizations, since solutions obtained in one field can be carried over to the other. However, considerable care has to be exercised in transforming the results of the theory of localization of electrons to the case of classical waves. The most important difference is that for classical waves, the equivalent of the particle number is not conserved. The quantity conserved here is the energy, leading to a diffusion behavior of the energy density. Another difference is that the scattering potential is frequency dependent as shown in eqn [6]. As a consequence, the energy transport velocity entering the diffusion coefficient for a strongly disordered system may be appreciably renormalized, and, as a result, diffusion coefficients can be quite small even far from the localization transition. In particular, the low values experimentally obtained for the diffusion coefficient, $D = v_E l/3$, are caused by extremely small values of the energy transport velocity, v_E, and not necessarily by the small values of l, which would signify strong localization. It is well understood that low values of v_E for classical waves are due to the Mie resonances of the scatterers. Near resonances, a lot of energy is temporarily stored inside the dielectric scatterer or, equivalently, the wave spends a lot of time (dwell time) inside the dielectric scatterer.

The outstanding problem in classical wave localization is to find the optimal conditions for its realization. It has been suggested that an intermediate frequency window of localized states separates the low-frequency extended states, characterized by Rayleigh scattering, from the high-frequency extended states, described by geometric optics. Theories based on weak scattering limit and on the coherent potential approximation (CPA) predict frequency intervals within which localization should be observed. These predictions are based on extrapolation of results obtained in the weak disorder regime. Wiersma *et al.*, in 1997, reported experiments at the near-infrared in GaAs powders, where the transmission coefficient, T, was measured in the extended, critical, and localized regimes. In the critical regime, T should vary with the inverse of the square of the sample thickness and in the localized regime, it should vary exponentially with the thickness. F Scheffold *et al.*, in 1999, argued that the results can be interpreted on the basis of the classical diffusion theory if absorption is included. One way to separate the effects of absorption and localization is to measure fluctuations of the transmission T, in addition to more conventional transport properties. This can be done easier at microwave frequencies, where one can measure both the amplitude and the phase of the electric field.

To facilitate the solution of the classical wave localization problem, it was proposed to construct first a periodic medium which, hopefully, will produce a spectral gap, and then by a disordering process, to create tails of localized states in this gap. The first part of this proposal produced much more than what one was looking for initially: it led to the creation of the so-called photonic (and phononic) band gap (PBG) artificial materials, and to the emergence of a new technological field.

See also: Disordered Magnetic Systems; Disordered Solids and Glasses, Electronic Structure of.

PACS: 71.23.−k; 71.23.An; 71.30.+h; 72.10.−d; 72.15.−v; 61.43.−j; 41.20.Jb; 05.60.Gg

Further Reading

Abrahams E, Kravchenko S, and Sarachik MP (2001) Metallic behaviour and related phenomena in two dimensions. *Reviews of Modern Physics* 73: 251.

Brandes T and Kettemann S (eds.) (2003) *Anderson Localization and its Ramifications*. Berlin: Springer.
Datta S (1995) *Electronic Transport in Mesoscopic Systems*. Cambridge: Cambridge University Press.
Economou EN (1983) *Green's Functions in Quantum Physics*, 2nd edn. Berlin: Springer.
Imry Y (2002) *Introduction to Mesoscopic Physics*, 2nd edn. Oxford: Oxford University Press.
Joannopoulos JD, Meade RD, and Winn JN (1995) *Photonic Crystals Molding the Flow of Light*. Princeton, NJ: Princeton University Press.
John S (1997) Frozen light. *Nature* 390: 661–662.
Kushwaha MS (1999) Bandgap engineering in phononic crystals. *Recent Research Developments in Applied Physics*. 2: 743–855.
Lifshits IM, Gredelkul SA, and Pastur LA (1998) *Introduction to the Theory of Disordered Systems*. New York: Wiley.
Sakoda K (2004) *Optical Properties of Photonic Crystals*, 2nd edn. Berlin: Springer.
Scheffold F, Lenke R, Tweer D, and Maret G (1999) Localization or classical diffusion of light? *Nature* 398: 206–207.
Soukoulis CM (ed.) (2001) *Photonic Crystals and Light Localization in the 21st Century*. Dordrecht: Kluwer.
Taylor PL and Heinonen O (2002) *A Quantum Approach to Condensed Matter Physics*, pp. 315–336. Cambridge: Cambridge University Press.
Wiersma DS, Bartolini P, Lagendijk A, and Righini R (1997) Localization of light in a disordered medium. *Nature* 390: 671–673.

Disordered Magnetic Systems

P Nordblad, Uppsala University, Uppsala, Sweden

Introduction

Disordered magnetic systems, when defined widely, comprises the whole field of applied magnetic materials – ranging from the extremely soft permalloy to the hardest permanent magnet as well as the physics of model systems of strongly disordered magnetic materials, spin glasses, and random-field Ising systems.

Magnetic ordering requires that the electron system forms local or itinerant magnetic moments and that there is interaction between these moments. Such interacting magnetic moments will eventually, as the temperature is lowered, become correlated and in certain cases form a long-ranged ordered phase at a critical temperature. The simplest magnetic order in crystalline systems arises when the leading interaction is ferromagnetic and there is only one type of magnetic ions in the material. The low-temperature phase then shows a regular pattern with the magnetic moments all aligned in parallel. Magnetic disorder in an ideal system of this type is enforced by thermal energy, and above the critical ordering temperature, a random paramagnetic phase forms. However, intrinsic quenched disorder, due to lattice dislocations, impurities, and other defects, always appears in a real magnetic system, also in the magnetically ordered phase. This kind of disorder is the key to the macroscopic magnetic properties of an ordered ferromagnet. The disorder and the microstructure of the system then determine if a weakly anisotropic magnet becomes a good soft ferromagnet or if a strongly anisotropic system attains applicable permanent magnetic properties. It is thus disorder, on nano- and micrometer length scales, that governs the quality of applied magnetic materials, whether soft or hard.

Models

A random distribution of the atomic magnetic elements in alloys and compounds introduces strong disorder and deviations from a regular interaction pattern. The interaction between the magnetic constituents becomes random in size and, in some cases, also in sign. This causes the appearance of new magnetic phases and phenomena. An interacting magnetic Ising system can be described by its spin Hamiltonian

$$H = -\sum_{i,j} J_{i,j} S_i S_j \qquad [1]$$

where $J_{i,j}$ is the exchange interaction strength between spin S_i and spin S_j: spins that in an Ising system point either up or down. A random-exchange ferromagnet is described if all $J_{i,j}$ are positive but of different magnitude, and a spin glass is described if the sign of $J_{i,j}$ varies but the mean value is zero. Equation [1] can be used to describe systems of any dimensionality and any range of interaction. Another important class of disordered magnetic Ising systems is the random field system

$$H = -\sum_{i,j} J_{i,j} S_i S_j + \sum_i h_i S_i \qquad [2]$$

where $J_{i,j}$ are positive interaction constants and h_i is a local field of random size and sign with zero mean that acts on spin number S_i. This system does not have an experimental realization, but a dilute Ising antiferromagnet in an applied homogeneous magnetic field has been shown to describe an equivalent problem:

$$H = -\sum_{i,j} J \varepsilon_i \varepsilon_j S_i S_j + H_a \sum_i \varepsilon_i S_i \qquad [3]$$